European Journal of Nuclear Medicine and Molecular Imaging (2019) 46:603–613
https://doi.org/10.1007/s00259-018-4180-3

ORIGINAL ARTICLE

Feasibility of multi-parametric PET and MRI for prediction of tumour recurrence in patients with glioblastoma

Michael Lundemann[1,2,3] · Per Munck af Rosenschöld[3,4] · Aida Muhic[5] · Vibeke A. Larsen[6] · Hans S. Poulsen[5] · Svend-Aage Engelholm[2,5] · Flemming L. Andersen[1] · Andreas Kjær[1,7] · Henrik B. W. Larsson[1] · Ian Law[1] · Adam E. Hansen[1]

Received: 19 April 2018 / Accepted: 21 September 2018 / Published online: 2 October 2018

Abstract

Background Recurrence in glioblastoma patients often occur close to the original tumour and indicates that the current treatment is inadequate for local tumour control. In this study, we explored the feasibility of using multi-modality imaging at the time of radiotherapy planning. Specifically, we aimed to identify parameters from pre-treatment PET and MRI with potential to predict tumour recurrence.

Materials and methods Sixteen patients were prospectively recruited and treated according to established guidelines. Multi-parametric imaging with ^{18}F-FET PET/CT and ^{18}F-FDG PET/MR including diffusion and dynamic contrast enhanced perfusion MRI were performed before radiotherapy. Correlations between imaging parameters were calculated. Imaging was related to the voxel-wise outcome at the time of tumour recurrence. Within the radiotherapy target, median differences of imaging parameters in recurring and non-recurring voxels were calculated for contrast-enhancing lesion (CEL), non-enhancing lesion (NEL), and normal appearing grey and white matter. Logistic regression models were created to predict the patient-specific probability of recurrence. The most important parameters were identified using standardized model coefficients.

Results Significant median differences between recurring and non-recurring voxels were observed for FDG, FET, fractional anisotropy, mean diffusivity, mean transit time, extra-vascular, extra-cellular blood volume and permeability derived from scans prior to chemo-radiotherapy. Tissue-specific patterns of voxel-wise correlations were observed. The most pronounced correlations were observed for ^{18}F-FDG- and ^{18}F-FET-uptake in CEL and NEL. Voxel-wise modelling of recurrence probability resulted in area under the receiver operating characteristic curve of 0.77 from scans prior to therapy. Overall, FET proved to be the most important parameter for recurrence prediction.

Conclusion Multi-parametric imaging before radiotherapy is feasible and significant differences in imaging parameters between recurring and non-recurring voxels were observed. Combining parameters in a logistic regression model enabled patient-specific maps of recurrence probability, where ^{18}F-FET proved to be most important. This strategy could enable risk-adapted radiotherapy planning.

Keywords Radiotherapy · Glioblastoma · Response prediction · FET · PET · MRI

Electronic supplementary material The online version of this article (https://doi.org/10.1007/s00259-018-4180-3) contains supplementary material, which is available to authorized users.

✉ Michael Lundemann
michael.juncker.lundemann@regionh.dk

1 Department of Clinical Physiology, Nuclear Medicine & PET, Rigshospitalet, University of Copenhagen, Copenhagen, Denmark

2 Department of Oncology, Section for Radiotherapy, Rigshospitalet, University of Copenhagen, Copenhagen, Denmark

3 Niels Bohr Institute, Department of Science, University of Copenhagen, Copenhagen, Denmark

4 Radiation Physics, Department of Hematology, Oncology and Radiation Physics, Skåne University Hospital, Scania, Sweden

5 Department of Oncology, Rigshospitalet, University of Copenhagen, Copenhagen, Denmark

6 Department of Radiology, Rigshospitalet, University of Copenhagen, Copenhagen, Denmark

7 Cluster for Molecular Imaging, Department of Biomedical Sciences, University of Copenhagen, Copenhagen, Denmark

Introduction

Radiotherapy in combination with chemotherapy after surgery remains the standard choice of treatment in patients with glioblastoma. However, the prognosis remains dismal, despite recent advancement in surgery [1], radiation dose delivery [2]

and availability of various chemo regimens [3]. The median time to progression is 7 months and median overall survival is 15 months [4]. Radiotherapy is conventionally planned on anatomical MRI and irrespective of regional differences in target definition [5]; the treated volume includes an up to 2–3 cm geometric expansion to include infiltrative tumour components, not evident on anatomical MRI [6]. This results in a large treatment volume, potentially including unaffected healthy tissue. The vast majority of tumour recurrences after radiotherapy occur within the treated high dose volume [7], indicating that the delivered dose is insufficient for local tumour control. Increasing the dose to the entire planning volume results in a high total brain dose, which may cause increased risk of toxicity [8]. Therefore, the possibility to define a more specific volume with a high risk of recurrence could be useful for an altered radiotherapy protocol. Definition of such a sub volume necessitates information beyond what is gained from conventional anatomical imaging and physiological and metabolic imaging have been proposed as viable supplement hereto. Diffusion weighted MRI (DWI), has been shown to correlate with cell density and integrity of tissue structure [9, 10]. The hemodynamic properties of the tumour can be assessed using perfusion MRI [11]. Dynamic contrast-enhanced (DCE) T1-weighted MRI has been shown as a feasible technique to measure vascular permeability (K_i), vascular blood volume (V_b), extra-vascular, extra-cellular blood volume (V_e), blood flow (F) and mean transit time (MTT) in a single acquisition [12]. Metabolic characterization of the tumour environment can be achieved using positron emission tomography (PET). PET employing radiolabelled amino acids, such as ^{11}C-L-methionine (MET) and ^{18}F-fluoroethyl-L-tyrosine (FET), has shown to increase accuracy of detecting glioma cells, when combined with conventional MRI [13, 14] and is a prognostic factor for both progression-free and overall survival [15]. In addition, studies have shown that tumours are likely to recur in the FET positive volume if not adequately treated [16]. Alterations of tumour energy metabolism, investigated with the use of ^{18}F-fluorodeoxyglucose (FDG) PET, have been shown to correlate with survival, despite the natural high glucose metabolism in normal appearing tissue [17].

In this study, we explored the feasibility of performing comprehensive multi-modal imaging of glioblastoma patients as part of their radiotherapy planning procedure. We aimed to identify imaging modalities that may predict tumour recurrence, by means of comparing multi-parametric PET and MRI before and after radiotherapy in a voxel-wise fashion. Finally, we wished to examine if multi-parametric PET and MRI could be used to establish a risk-model for predicting the voxel-wise probability of tumour recurrence. Ultimately, such models could enable patient-specific planning of dose delivery, tailored to specifically target areas with high risk of recurrence.

Materials and methods

Study design and patient selection

The study was conducted as a diagnostic, single-centre study including adult patients with histologically confirmed glioblastoma (WHO grade IV) (clinicaltrial.gov identifier: NCT02329795). The study was approved by the regional ethics committee (ID: H-3-2013-162). Patients were enrolled after surgery and exclusion criteria were: inability to undergo MRI examination, no written consent, ineligibility for standard regimen [18].

Image acquisition

Baseline scans were included from three imaging sessions performed approximately 1 week prior to start of radiotherapy; one routine MRI dedicated for radiotherapy planning (RT-MRI), one sequential ^{18}F-FET PET/CT, where the CT was used for radiation dose calculation, as well as PET attenuation correction, and one simultaneous ^{18}F-FDG PET/MRI. The RT-MRI and ^{18}F-FET PET/CT were usually carried out on the same day, with ^{18}F-FDG PET/MRI done on an alternative day within the same week. The MRI protocol included pre- and post-contrast T1, T2, FLAIR, diffusion tensor (DTI) and dynamic contrast-enhanced (DCE) perfusion imaging. Three-dimensional spectroscopic magnetic resonance imaging (MRSI) was performed, but the overall quality was not sufficient for analysis and will not be discussed further. Complete descriptions of acquisition parameters and data post-processing are provided in the appendix below. Total time in the scanner was approximately 70 min. RT-MRI was used for treatment planning only and is not used in the multi-parametric analysis. Identical imaging sessions including ^{18}F-FET PET/CT and ^{18}F-FDG PET/MRI were performed at the first follow-up approximately 3 months after the completion of radiotherapy. Only baseline images obtained prior to radiotherapy were analysed in this study.

Response assessment

Additional imaging beyond the 3-month follow-up was done every third month at local hospitals until the time of tumour recurrence. The local imaging protocols included as a minimum post-contrast T1, FLAIR and T2-weighted MRI. Radiographic progression was evaluated according to the RANO criteria [19]. In cases of suspected progression that did not meet the criteria according to RANO, a supplementary ^{18}F-FET PET was performed and decision on recurrence was made by a multidisciplinary tumour board, including neurosurgeons, neuro-radiologists, nuclear medicine physicians and neuro-oncologists. To address potential issues with pseudoprogression, i.e., treatment related changes that mimic

true tumour progression, relapse within the first 12 weeks after completion of radiotherapy had to be confirmed by re-operation or by the development in subsequent imaging sessions.

Treatment

Patients were treated with maximal safe tumour surgery, followed by adjuvant and concomitant chemo-radiotherapy [18]. Radiotherapy to 60 Gy was prescribed to the planning target volume (PTV), according to established guidelines [6]. Gross tumour volume (GTV) was delineated on RT-MRI and included the surgical cavity plus any remaining contrast enhancement on T1. A clinical target volume (CTV) margin up to 20 mm was added to the GTV and if necessary modified to include the FET-volume and exclude natural boundaries such as the skull. An additional 2 mm PTV margin was added to account for uncertainties in patient positioning. Daily image-guidance using stereoscopic X-rays and 6D patient positioning correction (ExacTrac and Robotics couch, BrainLab AG) was applied prior to each treatment. Chemotherapy with Temozolomide (TMZ) was prescribed daily with radiotherapy (75 mg/m^2) and subsequently up to six cycles in a 5-day schedule every 28 days (150–200 mg/m^2).

Regions of interest

Since the majority of glioblastoma patients recur within the treated volume, we restricted our analyses to image voxels within the CTV. Within CTV, voxels were separated into four regions of interest (ROIs); the contrast-enhanced lesion (CEL), the non-enhancing lesion (NEL), normal appearing white matter (WM) and normal appearing grey matter (GM). These four ROIs within the CTV formed the basis for all subsequent analyses. The CEL and NEL were semi-automatically delineated in ITK-SNAP (PICSL, Pennsylvania, PA, USA, http://www.itk-snap.org) [20] from hyperintense regions in the post-contrast T1 and FLAIR images, respectively. If present, the surgical cavity was delineated with reference to both the T2 and the pre-contrast T1. Any enhancement on the pre-contrast T1, indicating e.g. bleeding, was excluded from the CEL. The WM and GM were automatically segmentated in FSL (FMRIB, Oxford, UK; http://www.fmrib.ox.ac.uk/fsl/) using the T1 and FLAIR images [21].

The recurrent tumour volume (RV) was delineated using the Mirada Workstation (Mirada Medical, Oxford, UK) by a neuro-radiologist (VAL) and a nuclear medicine physician (IL), with reference to FLAIR, post-contrast T1 and FET obtained at the time of recurrence. In case no FET-PET was available at the time of recurrence, the RV was determined solely from FLAIR and post-contrast T1 and subsequently dilated by four pixels to match the resolution of the FET-PET.

Image registration

Pre-contrast T1 was selected as a common frame of reference and rigid registration using the ANTS toolbox [22] was used to align all other modalities. The registration parameters estimated for the CT was used to align the FET-PET.

Alignment of the RV was achieved through a sequential approach; the recurrence scan was registered to the reference T1 by an affine transformation, which was followed by a non-linear deformation. This was done to account for non-rigid deformations, especially apparent around the ventricles and surgical cavity. Non-linear deformations were estimated using the DRAMMS [23] toolbox, which automatically assigns a higher weight to image features that are present in both time points. This is desirable in registration of tumour images, as a one-to-one correspondence is not guaranteed. All imaging modalities, regions of interest and delineations were sub-sampled to 3x3x3 mm voxel size.

Parameter comparison and statistics

Within CTV, voxel-wise correlations between imaging parameters were assessed for each of the four ROIs (CEL, NEL, WM and GM) using Pearson's correlation coefficient. According to the outcome of the corresponding voxel in the recurrence scan, voxels were further divided into two subcategories: either as "recurring" or "non-recurring".

Empirical cumulative distribution functions with confidence bands were estimated for all voxels within each ROI and used to compare group differences in imaging parameters.

Differences in imaging parameters per patient were assessed by comparing the patient medians within each ROI using Wilcoxon's signed rank test. This was done to investigate if group differences were reproducible on a per-patient level.

Recurrence probability modelling

Voxel-wise binomial logistic regression models were used to create maps of tumour recurrence probability from the multi-parametric images obtained prior to radiotherapy. We assumed a different distribution of imaging parameters within each of the four tissue classes (WM, GM, CEL and NEL) within CTV and, thus, four separate binomial logistic regression models were established. For each model, the dependent variable was voxels at baseline that at the time of recurrence was either within the RV ("recurring") or outside the RV ("non-recurring"). The predictors were FET, FDG, mean diffusivity (MD), fractional anisotropy (FA), F, V_b, V_e, K_i, and MTT. All predictors were standardized to zero mean and unit variance. Model selection and model tuning is elaborated upon in the appendix below. Using a leave-one-out approach, four models were built using data from N-1 patients and subsequently used

to predict the tumour probability within each ROI in the remaining patient. This was repeated *N* times, leaving out a different patient in each iteration. The area under the receiver operating characteristic (ROC) curve (AUC) was used to assess model performance for voxel-wise prediction of tumour recurrence in each patient. The importance of each imaging parameter was assessed by evaluating the standardized logistic regression coefficients. Coefficients returned by the modelling procedure are related to the original scale of the predictors, hence the Agresti method [24] was used to standardize coefficients for comparison on a common scale.

Results

Patients

A total of 16 patients were enrolled in this study; however, one patient withdrew consent and is not considered further. Fourteen patients ($n = 14$) were classified as de novo glioblastoma (IDH1-wildtype) according to the 2016 molecular definition by WHO [25], and nine ($n = 9$) had methylated O^6-methylguanine-DNA methyltransferase (MGMT) promoter gene. All patient characteristics are shown in Table 1. One patient was unfit for concomitant TMZ due to low levels of thrombocytes, but his condition improved and received TMZ in the adjuvant setting after completing radiotherapy. Twelve of the 15 patients were available for analysis and the excluded patients were due to: death before first follow-up ($n = 1$), no imaging at time of recurrence (n = 1) and no evident recurrence at time of study (n = 1). Of the 12 evaluable patients, one patient developed meningeal carcinomatosis and was excluded, as the relapse mechanism is expected to differ substantially from the conventional relapse pattern. One patient recurred 12 weeks (124 days) after completion of radiotherapy and progression was subsequently confirmed by re-operation. For two patients, no baseline imaging was available due to technical issues ($n = 1$) and lack of patient compliance (n = 1). Thus, image acquisition was complete for nine patients in baseline and 10 patients at the first follow-up. The median time from surgery to baseline imaging was 20 (range: 15–43) days.

Treatment outcome

For the eligible patients, the median time to progression was 357 (range: 124–545) days and the overall survival was 631 (range: 290–766) days. A total number of 63,862 voxels within the CTV were available for analysis. Five patients had recurrence lesions outside the CTV. These lesions were excluded from analysis since the relapse mechanism is expected to differ from local recurrences. For the nine patients with evaluable baseline scans, recurrent tumour was registered in 6944 voxels within CTV. An overview of the number of voxels in the various ROIs is given in supplementary Table S1.

Table 1 Patient characteristics

Patient	Gender	Age at surgery (years)	MGMT-status	IDH-type	Surgery	WHO PS	Steroid usage[a]	Included in analysis	Recurrence	PFS (months)	OS (months)
1	F	54	met	wt	STR	0	Yes	No	Local	4	10
2	M	48	met	wt	GTR	0	No	Yes	Local and distant	17	25
3	M	58	met	wt	GTR	0	No	Yes	Local	9	14
4	M	44	non	wt	STR	0	Yes	Yes	Local and distant	13	22
5	M	53	non	wt	STR	0	No	No	Local	14	19
6	M	61	non	wt	GTR	0	No	No	Carcinomatosis	9	9
7	M	71	non	wt	STR	0	Yes	Yes	Local and distant	7	9
8	M	71	met	wt	GTR	0	No	Yes	Local	7	*25*
9	M	59	non	wt	GTR	0	No	Yes	Local and distant	13	15
10	F	68	met	wt	STR	1	Yes	No	Local	6	10
11	F	40	non	mut	STR	0	No	Yes	Distant	15	*21*
12	M	75	met	wt	GTR	1	Yes	No	No	4	4
13	M	67	met	wt	GTR	0	Yes	Yes	Local	4	*20*
14	F	70	met	wt	STR	0	No	Yes	Local	11	19
15	M	56	met	wt	GTR	0	Yes	No	No	*20*	*20*

Numbers in italic indicate censoring at the time of study.

[a] Steroid usage at the time of radiotherapy start

Abbreviations: *MGMT*, O^6-methylguanine-DNA methyltransferase; *met*, methylated: *non*, non-methylated; *IDH*, isocitrate dehydrogenase; *wt*, wildtype; *mut*, mutated; *STR*, subtotal resection; *GTR*, gross total resection; *PS*, performance status; *PFS*, progression free survival; *OS*, overall survival

Parameter comparison

An example of the acquired images is given in Fig. 1.

Pearson's correlation coefficients between imaging parameters within in each tissue class (WM, GM, CEL and NEL) are visualised in Fig. 2. A moderate to strong positive correlation is observed between most of the vascular parameters irrespective of the tissue class. Similarly, moderate to strong negative correlations are observed between MD and FA. For the two PET parameters, no correlation was found in normal appearing tissue, whereas strong positive correlations were found in CEL and NEL. Likewise, a moderate correlation was observed between the PET and vascular parameters in CEL and NEL only.

Figure 3 shows box and whiskers plots of patient medians within each tissue class for "recurring" and "non-recurring" voxels. Overall, the observed differences between "recurring" and "non-recurring" voxels were small, and no definitive threshold could be established for any of the parameters. Nonetheless, despite originating from the same tissue class in the baseline scan, there are significant median differences, dependent on whether the voxel recur or not. In general, voxels that are included in the RV at the time of recurrence show larger ^{18}F-FET-uptake when compared to voxels not included in the RV. This is irrespective of the originating tissue class (WM, GM, NEL or CEL). For the remaining parameters, there appears to be a tissue-dependent effect. Increased V_b, V_e, MTT and K_i were observed in WM, GM and NEL. For ^{18}F-FDG, an increased uptake is observed in recurring voxels that either originate from CEL or NEL, whereas voxels originating from GM show a reduced ^{18}F-FDG-uptake. For FA, an increase in fractional anisotropy for recurring voxels was observed for GM, CEL and NEL, whereas a reduction was found for WM voxels. Differences were statistically significant for ^{18}F-FDG-uptake within GM, CEL and NEL, ^{18}F-FET-uptake within all ROIs, FA within GM, MD within GM, MTT within WM, V_e within WM, and GM and K_i within WM and GM.

We compared the empirical cumulative distribution of imaging parameters for voxels pooled across all patients. The same overall pattern as described for the difference in median was observed. No absolute threshold on the parameters could be established, but distributions were visually different between "recurring" and "non-recurring" voxels for most parameters. The empirical cumulative distributions for imaging parameters are shown in supplementary Fig. S1.

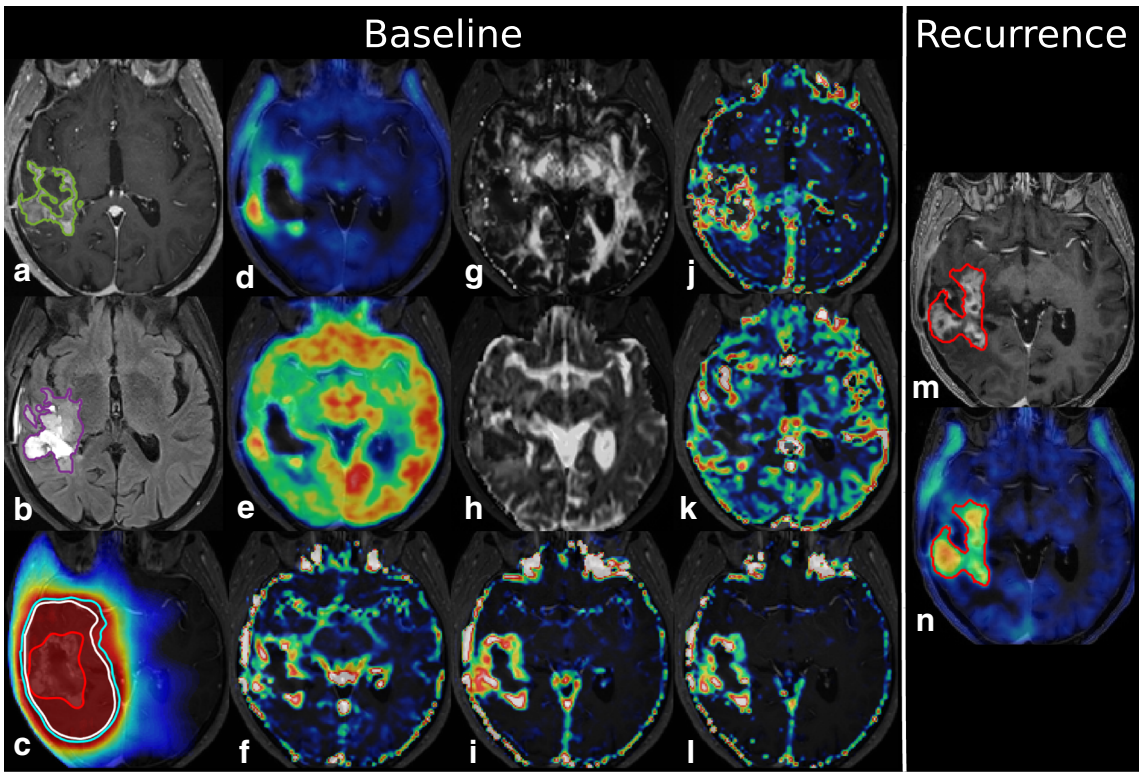

Fig. 1 Axial *baseline* (left) and recurrence (right) images from 70-year-old female with right temporal lope glioblastoma (patient 14). (**a**) contrast-enhancing lesion (green) from T1-weighted MRI, (**b**) FLAIR images showing non-enhancing lesion (purple), (**c**) radiotherapy dose plan with gross tumour volume (GTV) in red, clinical target volume (CTV) in white and planning target volume (PTV) in cyan, (**d**) ^{18}F-FET-uptake, (**e**) ^{18}F-FDG-uptake, (**f**) blood volume (V_b), (**g**) fractional anisotropy (FA), (**h**) mean diffusivity (MD), (**i**) extra-vascular, extracellular volume (V_e), (**j**) mean transit time (MTT), (**k**) blood flow (F), (**l**) vascular permeability (K_i), (**m**) recurrent tumour volume (RV) shown in red on contrast-enhanced T1-weighted MRI, (**n**) RV shown on ^{18}F-FET PET

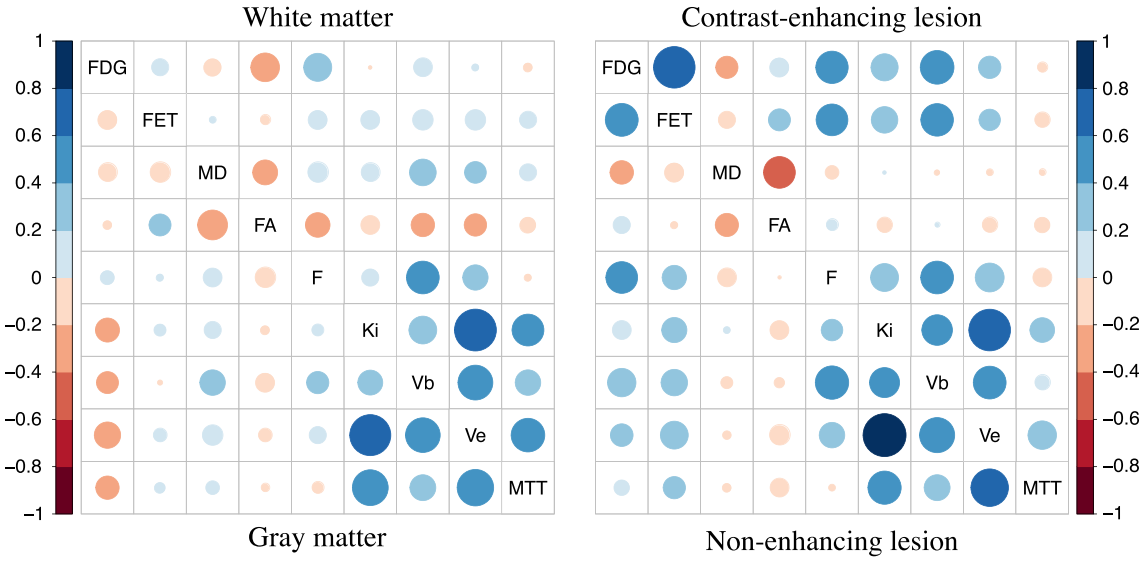

Fig. 2 Pearson correlation coefficient in different tissue classes within CTV for image parameters obtained prior to radiotherapy. Colour and size of circles indicate magnitude of correlation coefficient. As an example, for ^{18}F-FDG in white matter, a moderate negative correlation with FA and a moderate positive correlation with F were observed, as indicated by the red and blue circle in the top left row

Recurrence probability modelling

Binomial logistic regression models to predict the likelihood of recurrence were fitted using ^{18}F-FET-uptake, ^{18}F-FDG-uptake, MD, FA, F, V_b, V_e, K_i and MTT as predictor. Area under the ROC curves (AUC) for prediction of recurrence were 0.73, 0.78, 0.68 and 0.72 for voxels within WM, GM, CEL and NEL, respectively. Combining all models resulted in an AUC of 0.77. The recurrence probability maps within the CTV for all patients included in the analysis are shown in Fig. 4. The model was able to create a map of voxel-wise recurrence probabilities comparable with the recurrent tumour volume; however, notable patient variability was observed. For all models, the relative importance of predictor variables were estimated (shown in supplementary Fig. S2). Different imaging modalities were found to be important for prediction in different tissues; however, ^{18}F-FET-uptake had the highest relative importance in WM and GM and appeared as the overall most important parameter for recurrence probability modelling. High relative importance was also noted for ^{18}F-FDG-uptake and for varying vascular parameters in CEL and NEL. The relative importance of diffusion-derived parameters was generally low. However, FA was found to be second most important in healthy appearing tissue (both WM and GM).

Discussion

In this study, we explored the use of multi-parametric PET and MRI prior to radiotherapy for the location of tumour recurrence after radiotherapy in glioblastoma patients. The site of tumour recurrence was registered to pre-therapy imaging and several parameters, most notably those derived from ^{18}F-FET-PET, DCE-MRI and ^{18}F-FDG-PET, were found to be significantly different between voxels, which eventually did or did not recur. A predictive model for the voxel-wise likelihood of recurrence derived from pre-therapy imaging obtained an AUC of 0.77. Given the high risk of glioblastoma patients to currently recur within the planned high-dose volume, our study could be a first step to enable a higher degree of patient-specific planning of dose delivery by specifically targeting areas with high risk of recurrence.

Because of the use of two ^{18}F-labeled PET tracers, patients were to visit the hospital on two separate days both before and 3 months after completing radiotherapy. This setup complicated patient inclusion and underlines the importance to identify the most important imaging parameters. Moreover, an extensive PET/MRI protocol was used that required patient to be in the scanner for more than an hour. Despite this, patient compliance was high and only one of the commenced imaging sessions had to be aborted. Thus, we obtained a comprehensive set of data from a vulnerable population imaged at two difficult time points, and only spectroscopic imaging was discarded as the overall quality was too low for reliable analysis.

For ^{18}F-FET-uptake, we observed an increased uptake in voxels that later recurred, irrespective of the underlying tissue. Amino acid PET has been shown to identify the infiltrating parts of the tumour, which is characteristic for glioblastomas [13]. This is consistent with our observation of increased ^{18}F-FET-uptake in recurring WM and GM voxels. For ^{18}F-FDG-uptake in GM, we observed a significantly reduced uptake in voxels that later recurred, indicating a compromised cortical integrity, in agreement with a previous study reporting on a

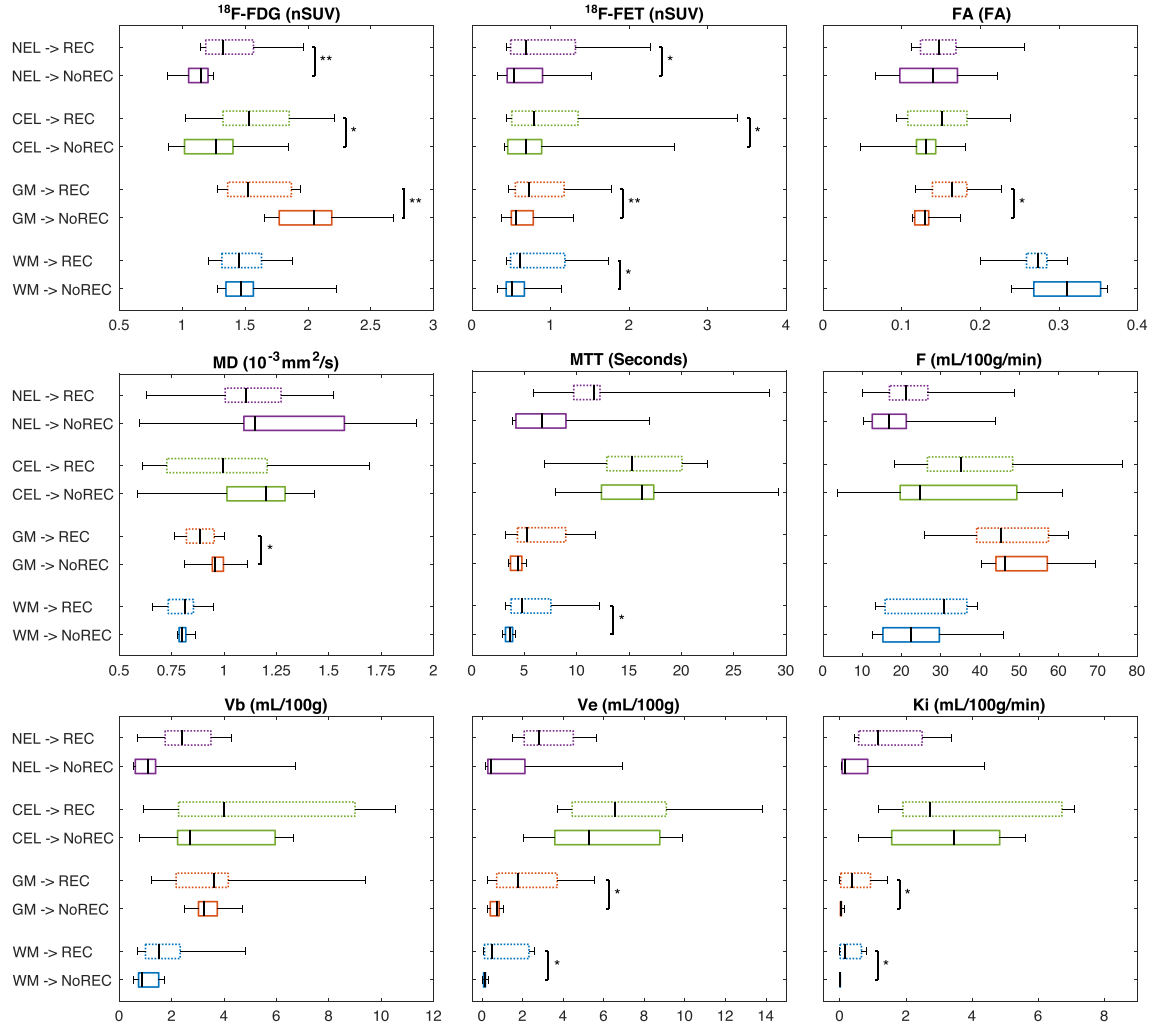

Fig. 3 Box and whisker plot of within-patient medians for imaging parameters within CTV in different tissue classes. WM: white matter (blue), GM: grey matter (red), CEL: contrast-enhancing lesion (green), NEL: non-enhancing lesion (purple). Regions are further separated dependent on outcome; either as within the recurrence volume (REC) represented by dashed boxes, or as outside the recurrence volume (NoREC) shown with solid boxes. The median (of patient medians) is represented by a black bar, boxes represent 1st to 3rd quantile and whiskers cover the data range. Wilcoxon signed rank test was used to compare medians. *: $p < 0.05$, **: $p < 0.01$

reduced ^{18}F-FDG-uptake in regions surrounding a local hotspot for tumours harbouring the cortex [26]. Likewise, we observed a significant increased ^{18}F-FDG-uptake within the abnormal CEL and NEL regions in voxels that later recurred, which correspond to the observation that a heterogeneous distribution of glucose transporters in glioblastoma cells may identify different habitats within the tumour [27]. These habitats may respond differently to both chemo- and radiotherapy and could explain the different treatment outcome. For recurring voxels, we observed a significant reduction in MD plus increase in FA in GM and a similar tendency in CEL and NEL, compatible with an increase in cell density as also previously reported in a biopsy-verified study on 20 patients with intracranial neoplasms [10]. Although not statistically significant, we furthermore observed a reduction in fractional anisotropy from DTI in otherwise normal-appearing white matter for recurring voxels, indicating a degradation of fibre integrity by infiltrating tumour, as also previously suggested [28]. With regard to perfusion metrics we observed a significant elevation of K_i and V_e for voxels in WM and GM that later recurred. This may indicate that subclinical neovascularization is ongoing already at the time of radiotherapy initiation which later manifest as visible tumour recurrence.

Patient-specific recurrence probability models were established, which achieved an AUC of 0.77 for voxel-wise prediction of recurrence from pre-therapy imaging. Few previous studies have tried to predict the site of recurrence from multi-modal imaging data. In a study with 15 similarly treated patients with tumours less than 5 cm in diameter, the authors used a histogram analysis of perfusion and diffusion metrics, but concluded that these two modalities were insufficient for predicting the site of recurrence [29]. In another recent study by Anwar et al. [30], employing also MRSI, but not PET, a comparable AUC of 0.75 for voxel-wise prediction was

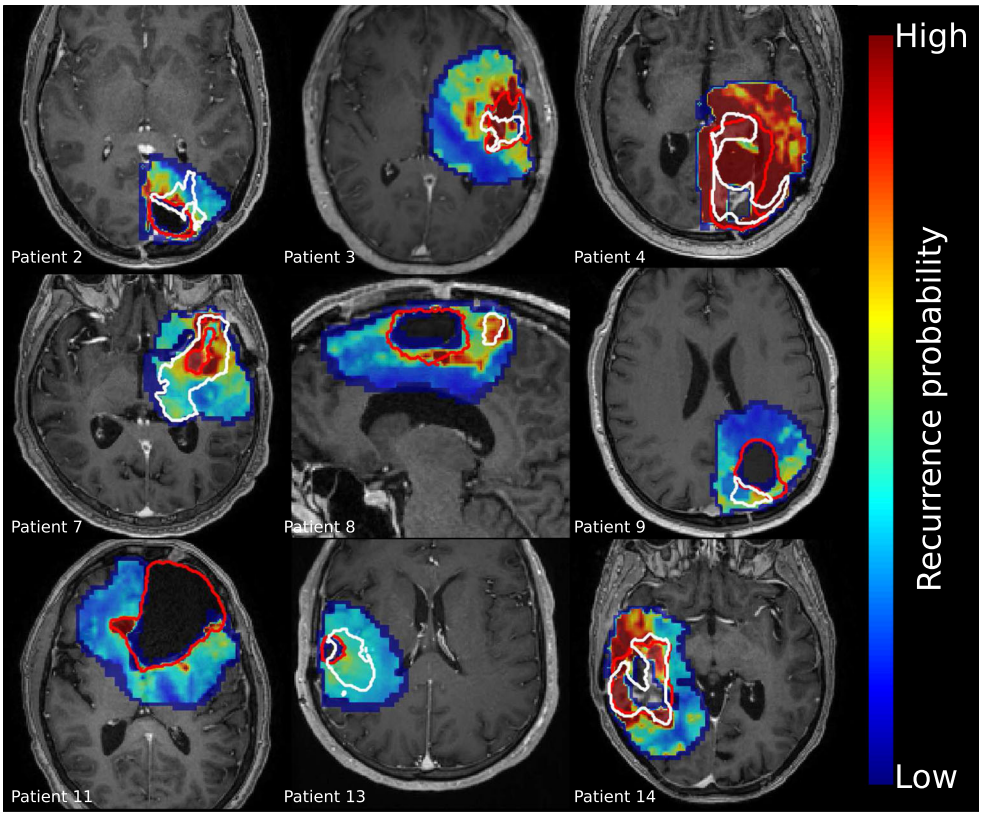

Fig. 4 Recurrence probability maps computed prior to radiotherapy overlaid on baseline T1-weighted MRI. The gross tumour volume (GTV) is shown in red and the actual recurrent tumour volume is shown in white. Patient 11 failed with a distant recurrence (thus, no in-field focus). Probability maps are scaled uniformly

found. However, the 24 patients were treated with an angiogenesis inhibitor, which may influence the performance of vascular parameters. Anwar et al. furthermore included dose and distance from the GTV as predictors, which makes a direct comparison with our study challenging. We focused exclusively on voxels within CTV that were treated with a uniform dose prescription and expect differences in dose to be less important for our study.

As our study employed two ^{18}F-labeled PET tracers and an hour-long PET/MR protocol, there is a need to identify the important and non-redundant image parameters, if the strategy is to be tested in a larger population. We observed a pattern of correlations among imaging parameters that depended on the underlying tissue. For the CEL and NEL regions, we observed a strong correlation between FET, FDG and the vascular parameters; however, no considerable correlation was found in WM and GM. This indicates that one or more may be omitted if the aim is to predict recurrence solely within the abnormal regions. When comparing the standardized coefficients from the recurrence models, we found FET to be a key parameter. This is supported by the significantly higher FET-uptake in baseline voxels within CTV that later recurred compared to voxels that did not recur, irrespective of the tissue (WM, GM, CEL or NEL). This may lead to the thought that ^{18}F-FET is appropriate for guiding dose-escalation; however, Piroth et al. failed to show any survival benefit in a small series of patients treated with 72 Gy to the ^{18}F-FET-positive volume. They further found that only approximately 30% of the RV occur within the baseline ^{18}F-FET-positive volume [31]. This overlap percentage was also found in our recent study [32] and indicates that ^{18}F-FET alone does not provide sufficient information for regional dose-escalation.

Based on the results obtained here, our recommendation for a simpler and manageable multi-parametric imaging protocol prior to radiotherapy would be PET/MRI (or PET/CT and 3T MRI) employing ^{18}F-FET PET, DCE-MRI and possibly DWI. This would require approximately 40 min of scan time in a PET/MRI scanner or 20 plus 40 min if separate PET and MRI scanners are used. The acquisition of combined ^{18}F-FET PET and perfusion using dynamic susceptibility contrast MRI has been shown to provide complementary diagnostic information [33, 34] and this may help to identify heterogeneous parts of the tumour.

There are a number of limitations to our study. Most importantly, the results presented are based on a low number of patients and needs further validation before the clinical utility can be tested in a prospective setting. However, the results are encouraging and serves as a starting point for further studies. Another limitation is the difference in spatial resolution of the acquired images and we expect some partial volume effects to be present in our data, especially for ^{18}F-FDG and ^{18}F-FET. This will be less of an issue for the median estimates within each patient, but could negatively influence the voxel-wise estimates and recurrence probability modelling. All imaging

modalities and regions of interest were subsampled to 3x3x3 mm to compensate for inaccuracies in image registration. This limits the level of spatial details of the recurrence predictions, but may to some extent also alleviate partial volume effects. Baseline scans were acquired approximately 3 weeks after surgery and this may influence the parametric images. Postoperative reactions, such as inflammation and other reactive changes, may lead to an increase in ^{18}F-FET- and ^{18}F-FDG-uptake, and surgical debris, including blood, may reside in the surgical cavity, which may affect the MRI signal in diffusion and perfusion measurements. We used a binomial logistic regression model for recurrence probability modelling, due to the binary outcome of a voxels at the time of recurrence. This model has the benefit of a probabilistic output, a pertinent feature if the strategy is to be used in a clinical trial. However, the model assumes a linear relationship between the predictors and the logarithmic odds of tumour recurrence, which may not necessarily be true. Other classification algorithms that do not have this assumption, such as support vector machines or neural networks, could be considered as alternatives. Importantly, the performance of the predictive model showed some patient dependence. This might be due to patient specific variability of imaging parameters which could not be modelled due to the relatively small number of patients included in this study. Furthermore, we experienced an unusually high fraction of patients with out-of-field recurrences (5/15) that could reflect a certain patient selection. However, since we focused our analyses on local recurrences, we expect this to play a minor role for the results presented.

Conclusion

Multi-modal imaging of glioblastoma patients as part of their radiotherapy workup proved feasible. Pre-therapy imaging showed significantly different median estimates between voxels that eventually did or did not recur for ^{18}F-FET-uptake, ^{18}F-FDG-uptake and perfusion-related parameters. A predictive model aimed at identifying voxels with high probability of tumour recurrence was built based on pre-therapy imaging parameters. The model obtained an AUC of 0.77 for voxel-wise prediction of recurrence within the CTV and could be potentially used for testing risk-adapted radiotherapy strategies.

Acknowledgements The authors would like to thank the John and Birthe Meyer Foundation for the donation of the Siemens mMR hybrid PET/MR system to Rigshospitalet. The authors would also like to thank Karin Stahr, Marianne Federspiel and Jakup Poulsen for help with data acquisition, Betina Rotbøll and Lotte S. Andersen for coordinating logistics and Kirsten Grunnet for clinical data management.

Funding This study was funded by the Lundbeck Foundation, Department of Oncology (Rigshospitalet), Department of Clinical Physiology, Nuclearmedicine & PET (Rigshospitalet) and the Niels Bohr Institute, Copenhagen University, Copenhagen, Denmark.

Compliance with ethical standards

Conflict of interest The authors declare that they have no conflict of interest.

Ethics statement All procedures performed were in accordance with the 1964 Helsinki declaration and approved by the ethical committee for the Capital Region of Denmark (H-3-2013-162).

Informed consent Informed consent was obtained from all individual participants included in the study.

Appendix

Imaging parameters

The ^{18}F-FET PET/CT was performed on a 64 slice Siemens Biograph mCT (Siemens, Erlangen, Germany) approximately 20 min after intravenous administration of 200 MBq FET. A spiral CT acquisition was immediately followed by 20 min static PET acquisition. CT images were reconstructed to a 512 × 512 matrix with a voxel size of 0.6 × 0.6 × 1 mm. PET images were reconstructed to a 400 × 400 matrix using 3D-OSEM with four iterations and 12 subsets and filtered with a 5 mm Gaussian filter to a nominal voxel size of 0.8 × 0.8 × 3 mm.

The ^{18}F-FDG PET/MRI was done on a Siemens Biograph mMR, with a 3 T magnet and 8-channel headcoil. A 60-min dynamic list-mode PET acquisition was performed simultaneously with the MRI acquisition after injection of 200 MBq FDG. An average of the PET frames from 40 to 60 min were reconstructed to a 344 × 344 matrix using OP-OSEM with four iterations and 21 subsets and filtered with a 3 mm Gaussian filter to a voxel size of 0.8 × 0.8 × 2 mm. The CT from the FET-PET/CT was used for attenuation correction [35]. Pre- and post-contrast 3D isotropic T1-weighted magnetization prepared rapid gradient echo (MPRAGE) were acquired with identical parameters; flip angle (FA) 9 degrees, echo time (TE) 2.52 ms, inversion time (TI) 900 ms, repetition time (TR) 1900 ms. The field-of-view was 256x256x208 in the APxISxRL direction with a resolution of 1x1x1 mm. Axial T2-weighted turbo spin echo with radial sampling (BLADE) was acquired with FA 90 degrees, TE/TR 117/9480 ms, 41 slices with a thickness of 3 mm and slice-gap of 0.9 mm, matrix size 320 × 320 with a 230 × 230 mm FoV resulting in 0.72 × 0.72 mm in-plane resolution. Fluid attenuated inversion recovery (FLAIR) images were acquired using axial T2-weighted turbo inversion recovery magnitude (TIRM) with FA 130 degrees, TE/TI/TR 58/2500/9000 ms, 50 slices with a thickness of 3 mm and no gap. The acquisition matrix was 256 × 256 and in-plane resolution of 0.45 × 0.45 mm.

Diffusion weighted images were acquired using an echo planar imaging (EPI) sequence with FA 90 degrees, TR/TE 4000/95 ms, 28 slices with a thickness of 3 mm and slice-gap of 0.9 mm, 128 × 128 matrix with 1.7×.1.7 mm in-plane resolution. Two diffusion weightings with b = 0 and b = 1000 s/mm^2 in 30 directions and four averages were used. In the last two averages the phase-encoding direction was reversed to enable restoration of image-distortions due to susceptibility differences. The DCE perfusion was acquired using a fast 3D spoiled gradient echo sequence with FA 14 degrees, TR/TE 3.63/1.02 ms, 30 axial slices, 180 time-frames and a temporal resolution of 2.6 s. Field-of-view was 187x230x150 in the APxRLxIS direction with a resolution of 2.4 × 2.4 × 5 mm. Images for T1-mapping were acquired before contrast injection using variable flip angles (8, 14 and 20, or 4, 8, 14 and 20 degrees) and otherwise identical parameters. Two half-dose (0.05 mL/kg) boluses of contrast agent (Gadovist 0.1 mmol/mL) were injected using a power injector approximately 18 and 85 s after the dynamic DCE acquisition was started.

Data processing

Diffusion tensor MRI was processed using FSL [36]. Data were first corrected for susceptibility induced distortions and eddy currents. Secondly, a diffusion tensor was fitted to each voxel resulting in maps of mean diffusivity (MD) and fractional anisotropy (FA). The DCE perfusion data was processed using in-house software written in MATLAB (The MathWorks, Inc., Natick, MA, USA) as described previously [12]. Shortly, the MRI signal was converted to relative signal time curves [37]. Blood flow (F) and mean transit time (MTT) were estimated using a model-free deconvolution regularized by Tikhonov's method [38]. Maps of vascular permeability (K_i), intravascular blood volume (V_b) and volume of the extra-vascular, extra-cellular space (V_e) were computed by fitting a two-compartment model to the concentration-time curves, with F fixed to the estimate from model-free deconvolution. The CT was used for attenuation correction of both FET and FDG [35]. Within each patient, ^{18}F-FDG-uptake was normalized to a manually defined healthy appearing region in centrum semi-ovale and ^{18}F-FET-uptake was normalized to healthy appearing contralateral cortex including grey and white matter using a standard method [14].

Binomial logistic regression model

Binomial logistic regression models were fitted using the lassoglm function in MATLAB (Statistics and Machine Learning toolbox, Matlab R2017a, The MathWorks, Inc., Natick, MA, USA) that implements a general linear model (GLM) with elastic net regularization. The regularization procedure has two hyperparameters, α and λ. The former reduces the effect of correlated variables, whereas the latter is adjusted to prevent overfitting. Five values for α and 100 different values for λ were investigated for each model and the optimal parameters were determined by 10-fold cross-validation with the objective to minimize binomial deviance. The α levels were selected from the set [0.05, 0.2, 0.5, 0.95, 1] and the experimental values for λ were automatically determined by lassoglm – see Friedman et al. [39] for details.

References

1. Stummer W, Pichlmeier U, Meinel T, Wiestler OD, Zanella F, Reulen H-J, et al. Fluorescence-guided surgery with 5-aminolevulinic acid for resection of malignant glioma: a randomised controlled multicentre phase III trial. Lancet Oncol. 2006;7:392–401.
2. Munck Af Rosenschöld P, Engelholm SSA, Ohlhues L, Law I, Vogelius I, Engelholm SSA. Photon and proton therapy planning comparison for malignant glioma based on CT, FDG-PET, DTI-MRI and fiber tracking. Acta Oncol. 2011;50:777–83.
3. Clarke JL, Molinaro AM, Phillips JJ, Butowski NA, Chang SM, Perry A, et al. A single-institution phase II trial of radiation, temozolomide, erlotinib, and bevacizumab for initial treatment of glioblastoma. Neuro-Oncology. 2014;16:984–90.
4. Stupp R, Hegi ME, Mason WP, et al. Effects of radiotherapy with concomitant and adjuvant temozolomide versus radiotherapy alone on survival in glioblastoma in a randomised phase III study: 5-year analysis of the EORTC-NCIC trial. Lancet Oncol. 2009;10:459–66.
5. Fogh S, Wahl M, Anwar M, Haas-Kogan D, Clarke JL, Sneed PK. Standardization and quality assurance of radiation therapy volumes for adults with high-grade gliomas. Semin Radiat Oncol. 2014;24:259–64.
6. Niyazi M, Brada M, Chalmers AJ, et al. ESTRO-ACROP guideline "target delineation of glioblastomas". Radiother Oncol. 2016;118:35–42.
7. Minniti G, Amelio D, Amichetti M, Salvati M, Muni R, Bozzao A, et al. Patterns of failure and comparison of different target volume delineations in patients with glioblastoma treated with conformal radiotherapy plus concomitant and adjuvant temozolomide. Radiother Oncol. 2010;97:377–81.
8. Lawrence YR, Li XA, el Naqa I, Hahn CA, Marks LB, Merchant TE, Dicker AP (2010) Radiation dose-volume effects in the brain. Int J Radiat Oncol Biol Phys 76:S20–S27.
9. Song SK, Sun SW, Ju WK, Lin SJ, Cross AH, Neufeld AH. Diffusion tensor imaging detects and differentiates axon and myelin degeneration in mouse optic nerve after retinal ischemia. Neuroimage. 2003;20:1714–22.
10. Kinoshita M, Hashimoto N, Goto T, Kagawa N, Kishima H, Izumoto S, et al. Fractional anisotropy and tumor cell density of the tumor core show positive correlation in diffusion tensor magnetic resonance imaging of malignant brain tumors. Neuroimage. 2008;43:29–35.
11. Jain R (2013) Measurements of tumor vascular leakiness using DCE in brain tumors: clinical applications. NMR Biomed 26:1042–1049.
12. Larsson HBW, Courivaud F, Rostrup E, Hansen AE. Measurement of brain perfusion, blood volume, and blood-brain barrier permeability, using dynamic contrast-enhanced T(1)-weighted MRI at 3 tesla. Magn Reson Med. 2009;62:1270–81.
13. Kracht LW, Miletic H, Busch S, Jacobs AH, Voges J, Hoevels M, et al. Delineation of brain tumor extent with [11C]L-methionine

positron emission tomography: local comparison with stereotactic histopathology. Clin Cancer Res. 2004;10:7163–70.
14. Pauleit D, Floeth FW, Hamacher K, Riemenschneider MJ, Reifenberger G, Müller H-W, et al. O-(2-[18F]fluoroethyl)-L-tyrosine PET combined with MRI improves the diagnostic assessment of cerebral gliomas. Brain. 2005;128:678–87.
15. Poulsen SH, Urup T, Grunnet K, Christensen IJ, Larsen VA, Jensen ML, et al. The prognostic value of FET PET at radiotherapy planning in newly diagnosed glioblastoma. Eur J Nucl Med Mol Imaging. 2017;44:373–81.
16. Lee IH, Piert M, Gomez-Hassan D, Junck L, Rogers L, Hayman J, Ten Haken RK, Lawrence TS, Cao Y, Tsien CI (2009) Association of 11C-methionine PET uptake with site of failure after concurrent temozolomide and radiation for primary glioblastoma multiforme. Int J Radiat Oncol Biol Phys 73:479–485.
17. Padma MV, Said S, Jacobs M, et al. Prediction of pathology and survival by FDG PET in gliomas. J Neuro-Oncol. 2003;64:227–37.
18. Stupp R, Mason WP, van den Bent MJ, et al (2005) Radiotherapy plus concomitant and adjuvant temozolomide for glioblastoma. N Engl J Med 352:987–996.
19. Wen PY, Macdonald DR, Reardon DA, et al. Updated response assessment criteria for high-grade gliomas: response assessment in neuro-oncology working group. J Clin Oncol. 2010;28:1963–72.
20. Yushkevich PA, Piven J, Hazlett HC, Smith RG, Ho S, Gee JC, et al. User-guided 3D active contour segmentation of anatomical structures: significantly improved efficiency and reliability. Neuroimage. 2006;31:1116–28.
21. Zhang Y, Brady M, Smith S. Segmentation of brain MR images through a hidden Markov random field model and the expectation-maximization algorithm. IEEE Trans Med Imaging. 2001;20:45–57.
22. Avants BB, Tustison NJ, Song G, Cook PA, Klein A, Gee JC. A reproducible evaluation of ANTs similarity metric performance in brain image registration. Neuroimage. 2011;54:2033–44.
23. Ou Y, Sotiras A, Paragios N, Davatzikos C. DRAMMS: deformable registration via attribute matching and mutual-saliency weighting. Med Image Anal. 2011;15:622–39.
24. Agresti A. Analysis of ordinal categorical data, 2nd ed. Wiley: Series in Probability and Statistics. 2010.
25. Louis DN, Perry A, Reifenberger G, von Deimling A, Figarella-Branger D, Cavenee WK, et al. The 2016 World Health Organization classification of tumors of the central nervous system: a summary. Acta Neuropathol. 2016;131:803–20.
26. Pirotte B, Goldman S, Massager N, David P, Wikler D, Vandesteene A, et al. Comparison of 18F-FDG and 11C-methionine for PET-guided stereotactic brain biopsy of gliomas. J Nucl Med. 2004;45:1293–8.
27. Labak CM, Wang PY, Arora R, Guda MR, Asuthkar S, Tsung AJ, et al. Glucose transport: meeting the metabolic demands of cancer, and applications in glioblastoma treatment. Am J Cancer Res. 2016;6:1599–608.
28. Price SJ, Jena R, Burnet NG, Hutchinson PJ, Dean a F, Peña a, et al. Improved delineation of glioma margins and regions of infiltration with the use of diffusion tensor imaging: an image-guided biopsy study. Am J Neuroradiol. 2006;27:1969–74.
29. Khalifa J, Tensaouti F, Lotterie JA, et al. Do perfusion and diffusion MRI predict glioblastoma relapse sites following chemoradiation? J Neuro-Oncol. 2016;130:1–12.
30. Anwar M, Molinaro AM, Morin O, Chang SM, Haas-Kogan DA, Nelson SJ, et al. Identifying voxels at risk for progression in glioblastoma based on dosimetry, physiologic and metabolic MRI. Radiat Res. 2017;188:303–13.
31. Piroth MD, Pinkawa M, Holy R, et al. Integrated boost IMRT with FET-PET-adapted local dose escalation in glioblastomas. results of a prospective phase II study. Strahlenther Onkol. 2012;188:334–9.
32. Lundemann M, Costa JC, Law I, Engelholm SA, Muhic A, Poulsen HS, et al. Patterns of failure for patients with glioblastoma following O-(2-[(18)F]fluoroethyl)-L-tyrosine PET- and MRI-guided radiotherapy. Radiother Oncol. 2017;122:380–6.
33. Henriksen OM, Larsen VA, Muhic A, Hansen AE, Larsson HBW, Poulsen HS, et al. Simultaneous evaluation of brain tumour metabolism, structure and blood volume using [18F]-fluoroethyltyrosine (FET) PET/MRI: feasibility, agreement and initial experience. Eur J Nucl Med Mol Imaging. 2016;43:103–12.
34. Verger A, Filss CP, Lohmann P, et al. Comparison of18F-FET PET and perfusion-weighted MRI for glioma grading: a hybrid PET/MR study. Eur J Nucl Med Mol Imaging. 2017;44:2257–65.
35. Andersen FL, Ladefoged CN, Beyer T, Keller SH, Hansen AE, Højgaard L, et al. Combined PET/MR imaging in neurology: MR-based attenuation correction implies a strong spatial bias when ignoring bone. Neuroimage. 2014;84:206–16.
36. Andersson JLR, Sotiropoulos SN. An integrated approach to correction for off-resonance effects and subject movement in diffusion MR imaging. Neuroimage. 2016;125:1063–78.
37. Saremi F. Perfusion imaging in clinical practice, a multimodality approach to tissue perfusion analysis. Hagerstown: Wolters Kluwer Health; 2015.
38. Larsson HBW, Hansen AE, Berg HK, Rostrup E, Haraldseth O. Dynamic contrast-enhanced quantitative perfusion measurement of the brain using T1-weighted MRI at 3T. J Magn Reson Imaging. 2008;27:754–62.
39. Friedman J, Hastie T, Tibshirani R. Regularization paths for generalized linear models via coordinate descent. J Stat Softw. 2010. https://doi.org/10.18637/jss.v033.i01.